Magnetic Stochasticity in Gyrokinetic Simulations of Plasma Microturbulence

W. M. Nevins, E. Wang, and J. Candy

Phys. Rev. Lett. **106**, 065003 — Published 10 February 2011

DOI: 10.1103/PhysRevLett.106.065003

Magnetic stochasticity in gyrokinetic simulations of plasma microturbulence

W.M. Nevins,[1] E. Wang,[1] and J. Candy[2]
[1]Lawrence Livermore National Laboratory, Livermore, California 94550
[2]General Atomics, San Diego, California 92121
(Received xx February 2010; …)

Analysis of the magnetic field structure from electromagnetic simulations of tokamak ion temperature gradient turbulence demonstrates that the magnetic field can be stochastic even at very low plasma pressure. The degree of magnetic stochasticity is quantified by evaluating the magnetic diffusion coefficient. We find that the magnetic stochasticity fails to produce a dramatic increase in the electron heat conductivity because the magnetic diffusion coefficient remains small.

DOI: PACS numbers: 52.35.Ra, 52.35.Vd, 52.30.Gz, 52.35.Qz

The most successful devices for confinement of fusion-grade plasmas are based on magnetic configurations, like tokamaks and stellarators, in which individual field lines cover nested toroidal surfaces. Recent stellarator designs place great importance on maintaining the integrity of these nested magnetic surfaces [1], while the integrity of the magnetic surfaces in tokamaks is a consequence of toroidal symmetry. Electromagnetic instabilities can spontaneously break the toroidal symmetry, thereby threatening the integrity of the magnetic surfaces [2]. The general view has been that spontaneous breaking of magnetic surfaces has dramatic consequences, e.g., the sawtooth crash and disruptions observed in tokamak discharges. In this letter we analyze the structure of the magnetic field in the presence of plasma microturublence, finding that turbulent magnetic perturbations break magnetic surfaces without producing dramatic consequences. This discovery requires that we adopt a more nuanced view of the magnetic field structure, quantifying the degree of magnetic stochasticity through the magnetic diffusion coefficient [3,4].

Recent advances in the development of gyrokinetic simulation codes have enabled high-resolution kinetic electromagnetic simulations of plasma microturbulence [5–8]. The importance of the perturbed magnetic field, included in electromagnetic simulations, relative to the corresponding electrostatic (no perturbed magnetic field) simulation depends on the dimensionless pressure [9], $\beta=8\pi p/B^2$, where p is the plasma pressure and B is the magnitude of the equilibrium magnetic field. At $\beta=0$ electrostatic modes are decoupled from magnetic perturbations. As β approaches m_e/M_i, where m_e and M_i are the electron ion masses respectively (about 0.05% in a hydrogen plasma) coupling to the shear component of the perturbed magnetic field becomes important. Generally, such coupling is found to be mildly stabilizing to ion temperature gradient (ITG) turbulence [10] because turbulent energy is diverted into bending magnetic field-lines. Field-line bending can result in deformations of magnetic flux surfaces; magnetic reconnection resulting in the formation of magnetic islands at the relatively high-order resonant surfaces associated with plasma microturbulence (that is, rational surfaces for toroidal mode numbers, n>>1); or, if the turbulent intensity is sufficient to cause island overlap [11], fracturing of magnetic surfaces and the appearance of magnetic stochasticity on the micro-scale (that is for length scales perpendicular to the magnetic field on the order of the sound radius, $\rho_s=(M_iT_e)^{1/2}/eB$, where T_e is the electron temperature and e is the magnitude of the electronic charge).

In this letter we report on an analysis of the magnetic field structure from a sequence of electromagnetic simulations [12] in which $\beta_e=8\pi n_eT_e/B^2$ is varied from 0 to 0.8%, where n_e is the electron density. We find that these electromagnetic simulations of ITG turbulence exhibit magnetic reconnection at surprisingly low values of β_e ($\beta_e \geq 0.1\%$), resulting in the destruction of essentially all magnetic surfaces within the simulation volume. The operating point for these simulations is based on the well-studied CYCLONE base case [13] with the addition of kinetic electrons and electromagnetic perturbations. That is, $R/a=2.775$, $r/a=0.5$, $T_e=T_i$, $R/L_{Te}=R/L_{Ti}=6.99$, $R/L_n=2.2$, $q=1.4$, $s=0.786$ and $\nu_{ei}=0$. Here R and a are the major and minor radii of the tokamak, while r is the radial location of the center of the flux tube; T_i is the ion temperature; L_{Te}, L_{ti}, and L_n are the radial scale lengths for the electron temperature, the ion temperature, and the density respectively; q is the magnetic safety factor while the logarithmic derivative of q, $s=(r/q)\partial q/\partial r$, describes the equilibrium magnetic shear; and ν_{ei} is the electron-ion collision frequency. In these simulations GYRO employed a 128-point velocity-space grid, (8 energies)×(8 pitch angles)×(2 signs of velocity), and 14 poloidal gridpoints per sign of velocity, together with 16 toroidal modes and 120 radial grid points, sufficient to resolve $k_\theta\rho_s$ up to 1.26 in increments of 0.105, and $k_x\rho_s$ up to 3.17 in increments of 0.106. We use kinetic electrons with $\mu\equiv(M_i/m_e)^{1/2}=42$, corresponding to a hydrogen plasmas, as this is less computationally expensive than a deuterium plasma

(μ=60) while the results are remarkably similar [12]. The dominant instability throughout this β-scan is the ITG mode, which liberates free energy mainly through ion heat transport. The turbulent ion heat conductivity, χ_i is more than three times larger than either the turbulent electron heat conductivity, χ_e, which in turn is about an order of magnitude higher than the turbulent particle diffusion coefficient, D, over the entire parameter scan. Both the maximum growth rate (over wave number) and the resulting ion heat transport decrease modestly as β_e is increased over the range $0.1\% \le \beta_e \le 0.8\%$ examined here [12].

The shear perturbation in the magnetic field is described by the parallel component of the vector potential, $A_{//}$. Magnetic reconnection occurs when the resonant component of $A_{//}$ has a finite value at its rational surface [14]. GYRO employs field-line following coordinates in which the poloidal angle, θ, is used to label position along $\boldsymbol{B}$. The resonant component of $A_{//}$ at the rational surface $r=r_{rat}(n)$, where n is the toroidal mode number, is then given by

$$A_\parallel^{res} = \langle A_\parallel(r=r_{rat}(n),n,\theta)\rangle_\theta .$$

The θ-average is taken over one poloidal circuit about the magnetic axis. We note that all rational surfaces of the fundamental mode of these simulations ($n=12$) are rational surfaces for every toroidal mode included in the simulation (that is, n's which are multiples of 12). Hence, an appropriate measure of the intensity of the resonant field at these fundamental rational surfaces is the resonant magnetic intensity,

$$\left\langle \left| \langle \delta A_\parallel \rangle_\theta \right|^2 \right\rangle_\alpha = \sum_{n\neq 0} \left| \langle A_\parallel(r,n,\theta,t) \rangle_\theta \right|^2$$

Figure 1 shows the resonant magnetic intensity plotted vs. (r, t). The fundamental rational surfaces are located at $r=2.97\rho_s$, $17.86\rho_s$, $32.74\rho_s$, and $47.62\rho_s$. Initial saturation of the linear ITG instability occurs at $t\approx 60\ a/c_s$. The resonant magnetic intensity does not vanish at the fundamental rational surfaces, indicating that magnetic reconnection has occurred. At issue is how this magnetic reconnection is manifested. The magnetic field might reconnect into a chain of islands localized about the rational surfaces and separated by regions in which the magnetic surfaces exist and are only slightly modified from the equilibrium magnetic surfaces. Alternatively, the ITG turbulence may cause widespread magnetic stochasticity. We investigate this issue by integrating along the perturbed magnetic field lines to produce the Poincaré surface-of-section plots shown in Fig. 2.

Modern gyrokinetic codes employ coordinates aligned with the equilibrium magnetic field. Generically, these coordinates involve two equilibrium field-line labels, α and β, together with a third coordinate, s, which labels

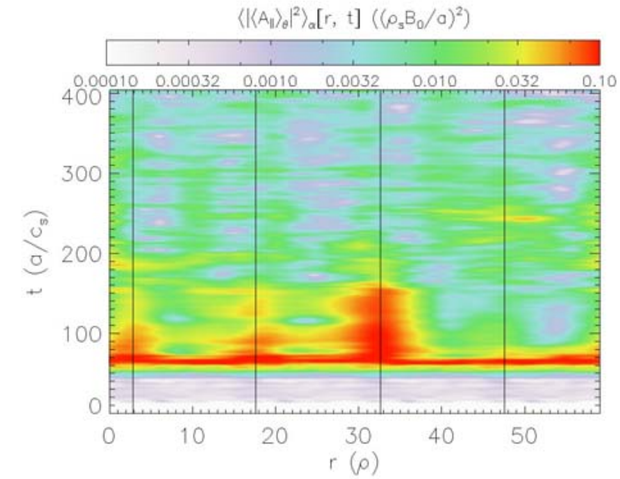

Fig. 1. The resonant magnetic intensity from a GYRO simulation at β=0.1%. Vertical lines show the fundamental rational surfaces at $r=2.97\rho_s$, $17.86\rho_s$, $32.74\rho_s$, and $47.62\rho_s$.

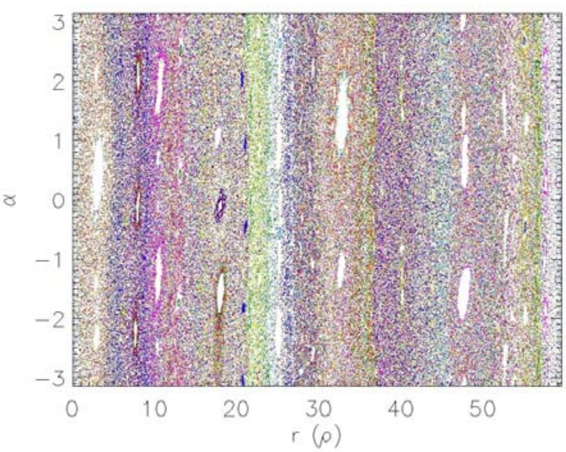

Fig. 2. A Poincaré surface-of-section plots for the GYRO simulation at β_e=0.1% and t=250, where individual field lines are denoted by their color.

position along the equilibrium field line. Field line trajectories satisfy the equations

$$\frac{ds}{B\cdot\nabla s} = \frac{d\alpha}{B\cdot\nabla\alpha} = \frac{d\beta}{B\cdot\nabla\beta}.$$

Consistent with the gyrokinetic ordering, we take $\delta\vec{B} = \nabla\times A_\parallel\hat{b} \approx \nabla A_\parallel\times\hat{b}$, yielding a Hamiltonian-like system of equations for the field line trajectories,

$$\frac{\partial\alpha}{\partial s} = \frac{1}{J\vec{B}\cdot\nabla s}\frac{\partial A_\parallel}{\partial\beta}\ ,\quad \frac{\partial\beta}{\partial s} = \frac{-1}{J\vec{B}\cdot\nabla s}\frac{\partial A_\parallel}{\partial\alpha}$$

where $J = 1/\left(\nabla\alpha\times\nabla\beta\cdot\hat{b}\right)$ is the Jacobian of our coordinate system. The field-line following coordinate system employed in GYRO is related to the usual poloidal (θ) and toroidal (φ) angles by choosing the first field-line label to be the Clebsch angle [15], $\alpha = \varphi + \upsilon(\psi,\theta)$, while the second field-line label, β, is related to be the poloidal flux, ψ. This choice has the useful property that the equilibrium magnetic field is given by $\vec{B}_0 = \nabla\alpha \times \nabla\psi$, while the field-line trajectories satisfy

$$\frac{\partial\alpha}{\partial s} = \frac{\partial A_{\|}}{\partial\psi}, \quad \frac{\partial\psi}{\partial s} = -\frac{\partial A_{\|}}{\partial\alpha}$$

where s is distance along the field. These equations must be supplemented by the appropriate periodicity condition, $\alpha \to \alpha \pm 2\pi q$ when a field line crosses the inboard mid-plane at $\theta = \pm\pi$, where the + (–) sign is used for crossings in which θ is increasing (decreasing). A Poincaré surface-of-section plot is formed by recording the locations where each field line crosses the outboard mid-plane of the simulation volume on successive poloidal cycles. If magnetic surfaces are regular, these points will lie on the field line's deformed (by the perturbed magnetic field) flux surface, while if the magnetic field is stochastic, these points will fill an area. It is clear from Fig. 2 that, even at $\beta_e = 0.1\%$, the magnetic component of the ITG turbulence destroys essentially all of the magnetic surfaces within the simulation volume. The field becomes stochastic during the initial saturation of the ITG instability ($t \approx 60\ a/c_s$), and remains stochastic throughout the remainder of the simulation.

Radial transport in gyrokinetic simulations can be divided into "electrostatic" transport, parameterized by χ_e^{ES} and describing electron radial heat transport arising from the radial component of the *ExB* velocity, and "magnetic flutter" transport, parameterized by χ_e^{EM} and describing electron radial transport arising from parallel streaming along the perturbed magnetic field yielding a radial velocity $v_{\|}\delta B_r/B_0$. The electron heat transport associated with magnetic stochasticity will appear as a component within the magnetic flutter transport. Over the range in β_e considered here the electrostatic electron heat transport, which varies from $\chi_e^{ES} \approx 2(\rho_s/a)\rho_s c_s$ to $\chi_e^{ES} \approx 3(\rho_s/a)\rho_s c_s$ as β_e varies from 0 to 0.8% [12], is always greater than the electron magnetic flutter heat transport, χ_e^{EM}. Figure 3 shows no dramatic increase in χ_e^{EM} with increasing β_e. On the contrary, χ_e^{EM} remains smaller than χ_e^{ES}, scaling as $\chi_e^{EM} \approx 1.9{\times}10^4 \beta_e^2 (\rho_s/a)\rho_s c_s$.

The absence of a dramatic increase in the electron heat transport when the magnetic field becomes stochastic at finite β_e can be explained in part by the very low intensity of the fluctuating magnetic field. The magnitude of the magnetic fluctuations associated with ITG turbulence is proportional to β_e [10] so that the stochastic magnetic transport [4], which is proportional to $(\delta B_r/B_0)^2$, is expected to scale as β_e^2.

The level of magnetic stochasticity can be quantified through the magnetic diffusion coefficient [4],

$$d_m = \lim_{\ell\to\infty} \frac{\left\langle [r_i(\ell) - r_i(0)]^2 \right\rangle}{2\ell} \approx \lim_{\ell\to\infty} \frac{1}{2\ell}\frac{1}{N}\sum_{i=1}^{N}[r_i(\ell) - r_i(0)]^2 \cdot$$

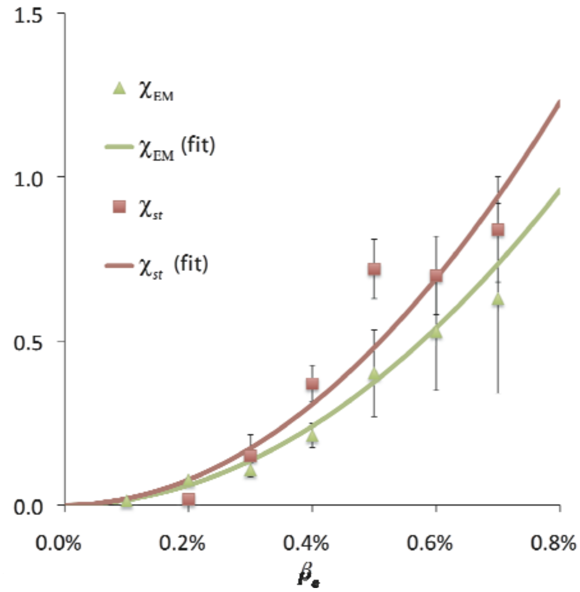

Fig. 3. The observed electron "magnetic flutter" heat transport (red squares) and the estimated of the stochastic electron heat transport (green triangles) are plotted against β_e. The error bars in both the magnetic flutter transport and the stochastic transport reflect the uncertainty in our estimate of the mean due to time variations over the simulation in question.

Where r_i is the radial position of the i^{th} field line, ℓ is the distance along the field line, and the average is to be taken over all magnetic field lines. We estimate the magnetic diffusion coefficient for representative time-slices from our simulations by following 100 magnetic field lines with initial positions distributed uniformly over the outboard midplane. Each field line is followed for 3000 of poloidal cycles. In the presence of a fully stochastic magnetic field our estimate of d_m goes to a well-defined limit after many poloidal cycles (Fig. 4).

The magnetic diffusion coefficient shown in Fig. 4, which has the dimensions of distance, is used to form the collisionless stochastic electron heat transport, $Q_e^{st} = -\chi_e^{st} n_e \partial T_e/\partial r$ with $\chi_e^{st} = 2 f_p \sqrt{2/\pi}\, v_{te} d_m$, following Ref. [16]. We have introduced the fraction of passing particles, $f_p \approx 1 - \sqrt{r/R}$, to account for the fact that magnetically trapped particles do not participate in the stochastic transport process described in Refs. [3], [4] and [16]. This expression for χ_e^{st} is based on questionable assumptions in the present case because the boundary conditions in our simulations require a vanishing radial average of the ambipolar electric field. Nevertheless, Harvey et als [16] expression for stochastic electron heat flux yields remarkable agreement with the simulation data as shown in Fig. 3. Work is underway to develop a more rigorous connection between the magnetic diffusion coefficient and the stochastic electron energy flux. The time-averaged stochastic electron heat transport plotted vs. β_e in Fig. 3 is obtained by evaluating d_m at many time slices over the simulation. Over the β_e–

scan reported here we find that χ_e^{st} scales with β_e as $\chi_e^{st} \approx 1.5 \times 10^4 \beta_e^2 (\rho_s/a)\rho_s c_s$.

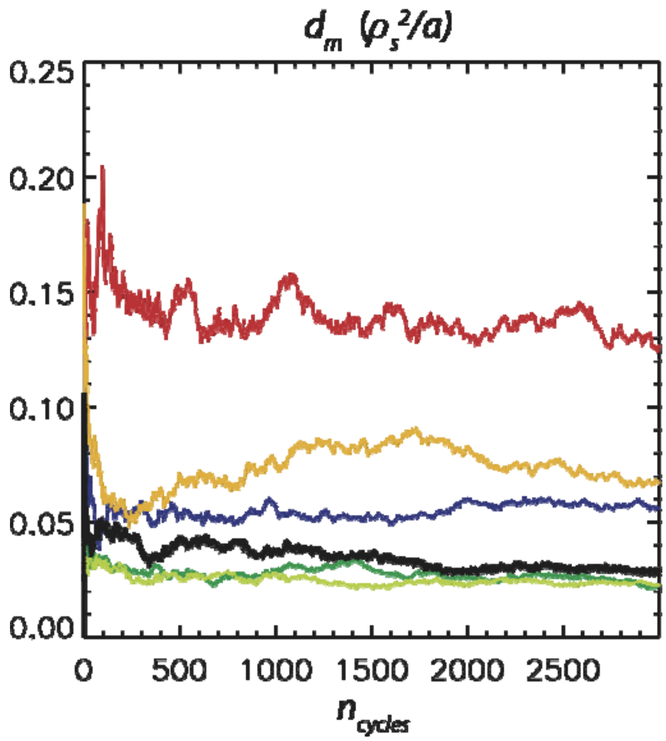

Fig. 4. The mean-squared radial field line displacement divided by twice the distance traveled along $\boldsymbol{B}$ for a gyro simulation with β_{e}=*0.6%* at *t=500 a/c*$_s$ (black curve), *t=450 a/c*$_s$ (red curve), *t=400 a/c*$_s$ (blue curve), *t=350 a/c*$_s$ (green curve), *t=300 a/c*$_s$ (chartruese curve), and *t=250 a/c*$_s$ (gold curve).

Our analysis of the microstructure of the magnetic field in a sequence of electromagnetic GYRO simulations of ITG turbulence yields the surprising result that the magnetic field becomes stochastic even at very low values of β_e ($\beta_e \geq 0.1\%$), much lower than the pressures observed in many tokamak experiments and those anticipated in magnetic fusion reactors. This suggests that magnetic stochasticity may be ubiquitous, motivating its quantification through the magnetic diffusion coefficient. The magnetic diffusion coefficient produced by the plasma microturublence is small enough that the stochastic electron heat transport does not result in a dramatic increase in the heat transport. Other important consequences of magnetic stochasticity remain to be investigated. For example, magnetic stochasticity gives rise to a radial conductivity $\sigma_r \approx \chi_e^{st}(\omega_{pi}^2/c_s^2)/2\pi$, resulting in damping of zonal flows at a rate $\gamma_Z \approx \frac{1}{2}\chi_e^{st}/\rho_s^2 \sim c_s/a$ for the magnetic diffusion coefficients observed in our simulations. Such rapid damping of zonal flows could profoundly affect the ability of zonal flows to regulate ITG turbulence [17] at finite β, and may responsible for the observed failure of the ITG turbulence to saturate in simulations at operating points like those considered here at only slightly larger values of β_e.

The authors gratefully acknowledge the National Center for Computational Sciences at ORNL for providing computer resources under INCITE award FUS023. We also acknowledge important conversations with M.J. Püschel, who has also demonstrated that plasma microturublence produces magnetic stochasticity over this beta-scan using the GENE code [18]. This work was performed under the auspices of the U.S. Department of Energy by Lawrence Livermore National Laboratory under Contract DE-AC52-07NA27344 and by General Atomics under contract number DE-FG03-95ER54309.

—

[1] see, *e.g.*, A.H. Boozer, Phys. Plasmas **5**, 1647 (1998).
[2] K.L. Wong, S. Kaye, D.R. Mikkelsen, J.A. Krommes, K. Hill, R. Bell, and B. LeBlanc, PRL **99**, 135003 (2007).
[3] M.N. Rosenbluth, R.Z. Sagdeev, J.B. Taylor, and G.M. Zaslavski, Nuclear Fusion **6** (4), 297 (1966).
[4] A.B. Rechester and M.N. Rosenbluth, PRL **40**, 38 (1978).
[5] J. Candy and R. E. Waltz, J. Comput. Phys. **186**, 545 (2003).
[6] W. Dorland, F. Jenko, M. Kotschenreuther, and B.N. Rogers, PRL **85**, 5579 (2000).
[7] Y. Chen and S. Parker, J. Comput. Phys. **189**, 463 (2003).
[8] A.G. Peeters, Y. Camenen, F.J. Casson, W.A. Hornsby, A.P. Snodin, D. Strintzi and G. Szepesi, Computer Physics Communications **180**, 2650 (2009).
[9] A.B. Mikhailovskii, "Theory of Plasma Instabilities" (Consultants Bureau, New York, 1974).
[10] J. Y. Kim, W. Horton, and J. Q. Dong, Phys. Fluids B **5** (11), 4030 (November, 1993).
[11] G.M. Zaslavsky and B.V. Chirikov, Sov. Phys. Usp. **14**, 549 (1972).
[12] J. Candy, Phys. Plasmas **12**, 072307 (2005).
[13] A. M. Dimits, G. Bateman, M.A. Beer, B.I. Cohen, W. Dorland, G.W. Hammett, C. Kim, J.E. Kinsey, M. Kotschenreuther, A.H. Kritz, L.L. Lao, J. Mandrekas, W.M. Nevins, S.E. Parker, A.J. Redd, D. E. Shumaker, R. Sydora, and J. Weiland, Phys. Plasmas **7**, 969 (2000).
[14] see, *e.g.*, F. L. Waelbroeck, Phys. Plasmas **10**, 4040 (2003).
[15] J. Candy, Plasma Phys. Control. Fusion **51**, 105009 (2009).
[16] R.W. Harvey, M.G. McCoy, J.Y. Hsu, and A.A. Mirin, PRL **47**, 102 (1981).
[17] P.H. Diamond, M.N. Rosenbluth, F.L. Hinton, M. Malkov, F. Fleischer, and A. Smolyakov, in *Plasma Physics and Controlled Nuclear Fusion Research*, 18th IAEA Fusion Energy Conference, Yokohama, Japan, 1998 (I.A.E.A., Vienna, 1999), pg. 1421.
[18] M.J. Püschel, Ph.D. Thesis, IPP Garching (Dec. 2009).